Energy & Environmental Science

Accepted Manuscript

ROYAL SOCIETY OF CHEMISTRY

www.rsc.org/ees

Journal Name

RSCPublishing

ARTICLE

Cite this: DOI: 10.1039/x0xx00000x

Received 00th January 2012,
Accepted 00th January 2012

DOI: 10.1039/x0xx00000x

www.rsc.org/

Hollow-tunneled Graphitic Carbon Nanofibers Through Ni-diffusion-induced Graphitization as High-performance Anode Materials

Yuming Chen,[a] Xiaoyan Li,[a] Xiangyang Zhou,[b*] Haimin Yao,[a] Haitao Huang,[c] Yiu-Wing Mai[ad] and Limin Zhou[a*]

N-doped nanoporous graphitic carbon has been attracting great interest because of its distinctive structure and physical properties. In this paper, we exploited a novel method to control Ni-induced graphitization by diffusing Ni nanoparticles from graphitic carbon spheres into N-doped amorphous carbon nanofibers, which turns amorphous carbon into graphitic carbon and produces a hollow-tunnel structure in electrospun carbon/Ni nanofibers. The resultant materials were further treated by chemical activation and acid treatment to develop activated N-doped hollow-tunneled graphitic carbon nanofibers (ANHTGCNs). In a typical application, we demonstrate that ANHTGCNs are excellent anode materials for lithium ion batteries (LIBs), displaying a superhigh reversible specific capacity of ~1560 mAh g^{-1} and a remarkable volumetric capacity of ~1.8 Ah cm^{-3} at a current density of 0.1 A g^{-1} with outstanding rate capability and good cycling stability.

Introduction

Nanoporous carbon materials have attracted considerable technological interest owning to their numerous applications, including improving the tensile strength of composites,[1] as catalyst and sensor supports,[2-5] as hydrogen-storage materials,[6] and in electronic and electrochemical devices.[7-9] Template-based processes have traditionally been the main methods of synthesizing porous carbon materials with large surface areas.[10] For example, ordered mesoporous amorphous carbon has been synthesized by using ordered silica as a template.[11] The introduction of sacrificial polymers such as poly(methyl methacrylate) (PMMA) and poly-L-lactic acid (PLLA) into polyacrylonitrile (PAN) solution creates pores in amorphous carbon nanofibers (ACNFs) by thermal treatment for eliminating these sacrificial polymers during carbonization of PAN.[12, 13] Additives such as KOH and $ZnCl_2$ also serve as activating agents to form porous structures.[14, 15] However, the degree of graphitization of these porous carbon materials is very low. To improve the graphitization of porous structures, we successfully utilized nickel nanoparticles to graphitize amorphous carbon into graphitic carbon and dissolved the Ni particles to produce hollow graphitic carbon nanospheres with different hollow diameters by electrospinning technology.[16, 17] ACNFs or amorphous carbon nanotubes (ACNTs) can be decorated with a hollow graphitic structure to obtain hybrid porous carbon materials with a high conductivity. Recent work has shown that graphitic porous CNFs can be fabricated by a chemical vapor deposition (CVD) approach by using a graphene/cobalt substrate.[18] Nitrogen-doping also generates extrinsic defects in graphitic carbon materials (graphene and CNT);[19, 20] the materials thus obtained show outstanding electrical and electrochemical properties. However, despite these advantages, these methods have yet to produce a good combination of pore size, pore number control, N-doping, and a high degree of graphitization. It is thus of merit to explore and develop a novel approach to the preparation of controlled N-doped porous graphitic carbon nanomaterials.

This study used PAN with a high N content (~26.4 wt. %) as a typical N-doped carbon precursor, Ni formed by the decomposition of nickel acetate ($Ni(Ac)_2$) as a normal catalyst for the graphitization of PAN, and PMMA as a sacrificial component to produce the pores. We controlled the Ni-induced graphitization by diffusing Ni

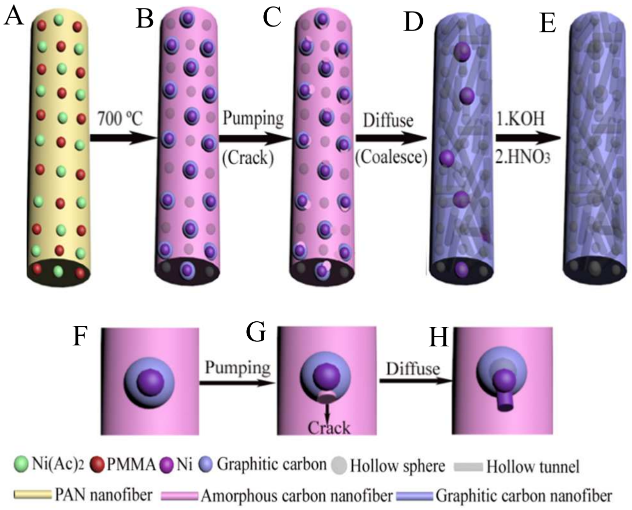

Figure 1. Schematic of material processing. (A) PAN/$Ni(Ac)_2$/PMMA composite nanofiber; (B) N-doped hollow-sphere carbon/Ni nanofiber (NHSCNN); (C) N-doped hollow-sphere carbon/Ni nanofiber, where the graphitic layers are cracked; (D) N-doped hollow-tunneled graphitic carbon/Ni nanofiber (NHTGCNN); (E) Activated N-doped hollow-tunneled graphitic carbon nanofiber (ANHTGCN). (F-H) Magnified images of (B-D).

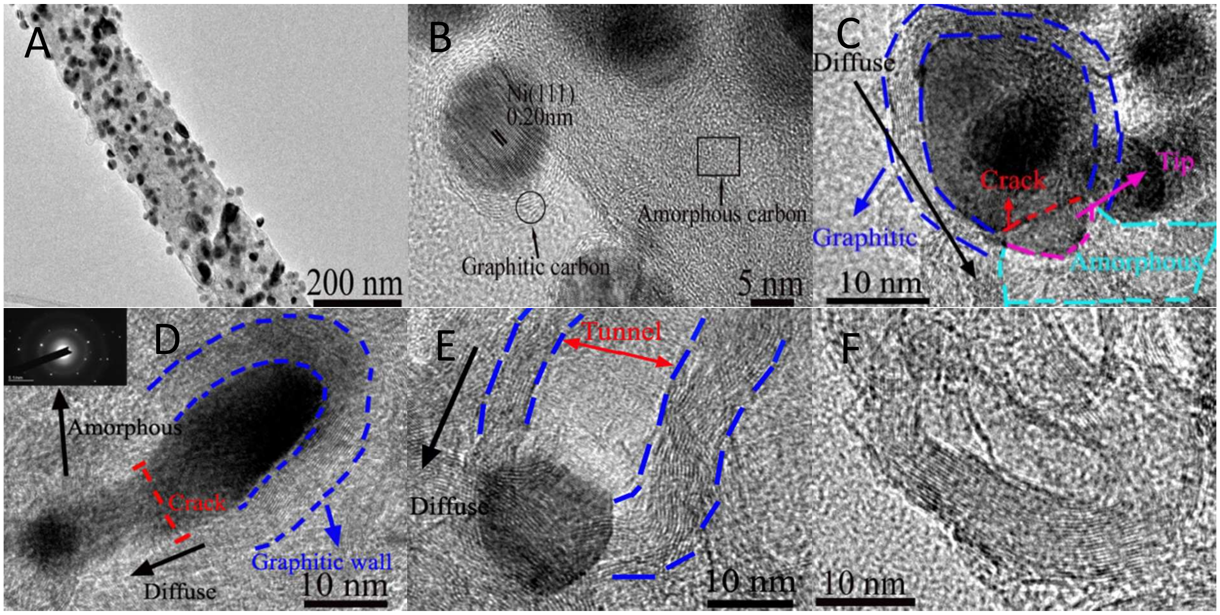

Figure 2. TEM and HRTEM images of N-doped carbon/Ni nanofiber (NCNN) (A, B) by calcining PAN/Ni(Ac)$_2$ composite nanofibers in Ar for 6 h, and NHTGCNN by calcining NCNN at 700 °C with subsequent sudden pumping to the vacuum of ~ -750 Torr which was maintained for 1 min (C), 5 min (D), 2 h (E), and 6 h (F), respectively.

nanoparticles from graphitic carbon spheres into N-doped amorphous carbon nanofibers, thereby turning amorphous carbon into graphitic carbon and producing a hollow-tunnel structure in electrospun carbon/Ni nanofibers. The resultant materials were further treated by chemical activation and acid treatment to create a novel architecture of activated N-doped hollow-tunneled graphitic carbon nanofibers (ANHTGCNs). Among the many potential applications for nanostructured carbon materials with N-doping, plentiful pores, and a high surface area, lithium ion batteries (LIBs) are demonstrated here as a typical example. The ANHTGCNs show a superhigh reversible capacity of ~ 1560 mAh g^{-1} with a remarkable volumetric capacity of ~1.8 Ah cm^{-3} at a current density of 0.1 A g^{-1}, outstanding rate capability, and good cycling stability.

Experimental

Preparation of activated N-doped hollow-tunneled graphitic carbon nanofibers (ANHTGCNs).

The outer fluid was a mixture of polyacrylonitrile (PAN, 1.5 g, MW=150 000, Aldrich) and nickel acetate (Ni(Ac)$_2$·4H$_2$O, 1.5 g, Advtechind) in 29.5 mL of dimethylformamide (DMF, Aldrich). Poly(methyl methacrylate) (PMMA, Tokyo Chemical Industry Co., Ltd) solution was used as the inner fluid. The solution was prepared by dissolving 1.5 g of PMMA in 30 mL of dimethylformamide (DMF) solvent. The set-up for the coaxial electrospinning is shown in Figure S1†. In brief, the spinneret consisted of coaxial stainless-steel tubes. The distance between the cathode and anode was maintained at 20 cm and a high voltage of 21 kV was applied to the syringe needle tip and the metal collector using a power supply. The typical feeding rate for the coaxial solutions was set at 0.04 mm/min (KATO Tech Co., Ltd). The as-collected electrospun fibers were stabilized at 250°C for 2 h and then carbonized at 700°C in a tube furnace connected with pumping valves for the sudden pumping to a vacuum of ~-750 Torr, which was maintained for 6 h (the vacuum was controlled by quickly switching the valve on and off) to obtain N-doped hollow-tunneled graphitic carbon/Ni nanofibers (NHTGCNNs). The heating rate was fixed at 5 °C/min. For the preparation of the ANHTGCNs, 480 mg of NHTGCNNs was dispersed in 20 mL of 7 M KOH solution and stirred for 12 hours followed by another 24 hours of static soaking in ambient conditions. The mixture was filtered through a polycarbonate membrane to remove the extra KOH solution and the NHTGCNNs/KOH mixture was then dried in a vacuum at 60°C for 24 hours. The dry precursor NHTGCNNs/KOH was first heated at 250°C for 30 minutes, and then treated at 700°C for 1 hour in a tube furnace under a nitrogen atmosphere. The activated mixture was washed by deionized water and further treated with HNO$_3$ at room temperature to obtain the ANHTGCNs.

Characterization

The morphology of the prepared materials was examined with a JEOL 2100F TEM (JEOL, Japan) with an Electron Energy Loss Spectroscopy (EELS) spectrometer (Gatan, Enfina). The X-ray photoelectron spectroscopy was used to evaluate the elemental compositions (XPS, PHI5600). Raman spectroscopy of all of the samples was obtained by a Jobin-Yavon T6400 micro-Raman system with an Ar$^+$ laser. N$_2$ adsorption and desorption isotherms at 77 K were identified by using a Micromeritics, ASAP2020 analyzer.

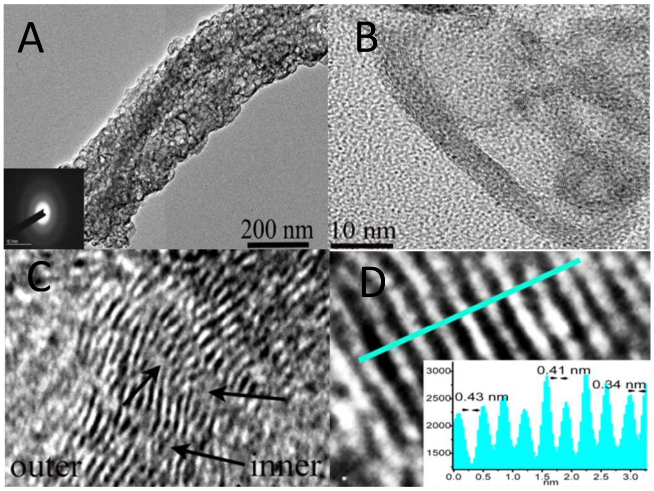

Figure 3. Morphology and structure of the materials. TEM and HRTEM images of ANHTGCNs (A), hollow-tunnel structure (B), the wall of hollow structure (C) and d-spacing distribution of graphene sheets and line profiles (inset) extracted from the image (D).

The pore-size distribution was calculated using the non-local density functional theory (NLDFT) method.

Electrochemical test

The electrochemical measurements were evaluated by cycling 2032 coin cells with the mixed materials (the prepared sample (80 wt.%), carbon black (10 wt.%), and poly(vinyl difluoride) (10 wt.%, PVDF)) as the working electrode and lithium metal foil as the counter/reference electrode. The test electrode was prepared by pasting the mixed materials onto copper foil. The electrolyte was a 1M solution of $LiPF_6$ in a 1:1 vol/vol mixture of ethylene carbonate (EC) and diethyl carbonate (DEC). Celgard 2400 film was used as the separator film. The charge (lithium insertion) and discharge (lithium extraction) were conducted with an Arbin automatic battery cycler at several current densities between the cut-off potentials of 0 and 3 V.

Results and discussion

Synthesis and characterization of ANHTGCNs.

We used a typical coaxial electrospinning method to obtain the ANHTGCNs. As shown in Figure S1†, two viscous liquids were simultaneously fed through the inner PMMA and outer mixture of PAN and $Ni(Ac)_2$ metallic capillaries. When a suitably high voltage of 21 kV was applied between the spinneret and the collector, the jet was stretched by electrostatic forces. The PAN and PMMA were mixed together during the electrospinning process as the same DMF solvent was used.[21] Hence PMMA could be distributed in the PAN matrix and $PAN/Ni(Ac)_2/PMMA$ composite nanofibers were prepared (Figure 1A). The collected nanofibers were then stabilized at 250ºC for 2 h and pyrolyzed at 700ºC by sudden pumping from ordinary pressure to a vacuum of ~ -750 Torr for 6 h by quickly switching the pumping valve on and off. The PMMA decomposed completely to create pores, and Ni nanoparticles were formed by the decomposition of the $Ni(Ac)_2$, and N-doped amorphous carbon carbonized from PAN on the surface of the Ni nanoparticles was graphitized into N-doped graphitic carbon under the catalytic effect of Ni (Figure 1B).[17] When the vacuum of ~ -750 Torr was suddenly applied, the carbon/Ni composite nanofibers expanded. Due to the difference in expansibility of the three phases (amorphous carbon, graphitic carbon, and Ni particle),[22, 23] a large stress was generated at the interfaces of the phases, cracking the graphitic layer (Figure 1C, G).[24] The Ni then diffused out of the nanoparticles via the crack (Figure 1H) and coalesced, creating a hollow-tunnel structure and further graphitizing the amorphous carbon into graphitic carbon during the Ni diffusion process. Figure 1D shows the resulting N-doped hollow-tunneled graphitic carbon/Ni nanofibers (NHTGCNNs) fabricated through the above process. Finally, ANHTGCNs with a tap density of ~0.3 g/cm^3 were prepared by a combination of KOH activation and HNO_3 treatment (Figure 1E). To clearly explain the proposed mechanism of Ni diffusion, we prepared several typical samples under different conditions for comparison (Table S1†). Sample 1 (N-doped carbon/Ni nanofibers, NCNNs) was prepared by calcining $PAN/Ni(Ac)_2$ composite nanofibers in Ar at 700ºC for 6 h (Figure 2A, B). Sample 2 was fabricated by adjusting the vacuum of the tube furnace to ~ -750 Torr by pumping at room temperature and then calcining the NCNNs at 700°C for 0.5 h (Figure S3A, *B*†). Sample 3 was obtained by calcining the NCNNs at 700°C with subsequent slow (0.5 h) pumping to a final vacuum of ~ -750 Torr (Figure S3C, D†). Sample 4 was prepared by calcining the NCNNs at 700°C with subsequent rapid pumping to a final vacuum of ~ -375 Torr, which was then maintained for 0.5 h (Figure S3E, F†). Samples 5 and 6 were obtained by directly calcining (sample 5, Figure S3G†) $PAN/Ni(Ac)_2$ composite nanofibers or (sample 6, Figure S3H†) $PAN/Ni(Ac)_2/PMMA$ composite nanofibers at 700 °C with sudden pumping to a final vacuum of ~ -750 Torr, maintained for 6 h and controlled by rapidly switching the pumping valve on and off.

To investigate the structures produced, transmission electron microscopy (TEM) and high-resolution TEM (HRTEM) images of the synthesized materials were taken. Figure 2A.B shows TEM and HRTEM images of sample 1. Metallic Ni nanoparticles catalyzed the amorphous carbon into graphitic carbon to give ACNFs containing Ni nanoparticles encapsulated in graphitic carbon nanospheres with a thickness of ~5 nm as compared with ACNFs (Figure S2A, B†).[16] Figures S3† and S4† show TEM and HRTEM images of various typical carbon/Ni nanofibers obtained under different experimental conditions. It is clear that the Ni nanoparticles could not diffuse from the graphitic carbon spheres into the amorphous carbon nanofibers (samples 2 and 3; Figure S3A-D†). Furthermore, the small pressure difference from ordinary pressure to ~ -375 Torr by sudden pumping was not suitable for the diffusion of Ni nanoparticles (sample 4, Figure S3E, F†). However, the Ni nanoparticles easily diffused into the amorphous carbon nanofibers by sudden pumping to vacuum of ~ -750 Torr at 700ºC (Figure S4†). This diffusion occurred owning to the expansion of the composite nanofibers when a large difference pressure (~-750 Torr) was suddenly applied at 700ºC. Because of the difference in expansibility of the three phases, a large stress was generated among the interfaces sufficient to deform the graphene sheets, thereby causing the cracking of the graphitic layer.[24] This led to the diffusion of Ni particles from the crack (Figure 2C, D). It was clear that very little Ni first diffused from the crack caused by the high pressure difference to form a tip (Figure 2C). As the diffusion of Ni further proceeded, the size of crack increased and the morphology of Ni changed from a sphere into an elongated shape. The carbon on the surface of tip of Ni particle was still amorphous carbon, which can be further proved by the SEAD pattern (inset) showing no clear ring-like pattern corresponding to graphitic carbon (Figure 2D). The carbon on the surface of the Ni particle was graphitic carbon, shown by blue arrow, indicating that it needs some time for graphitization. Second, the elongated Ni turned

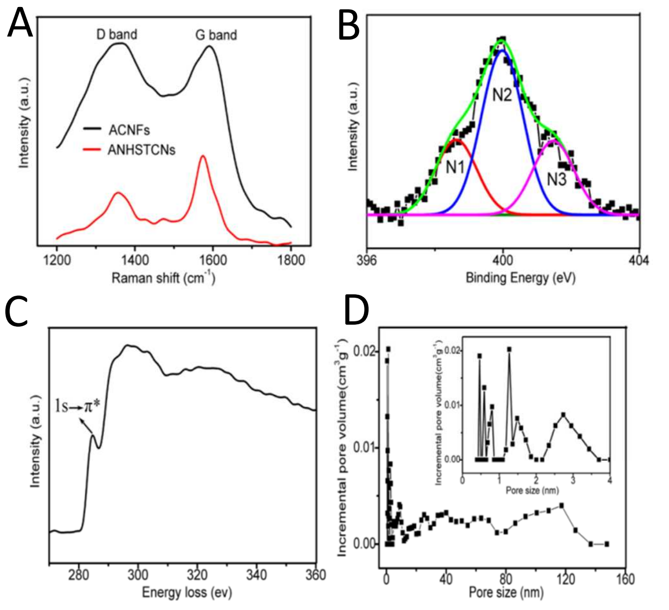

Figure 4. Characterization of materials. (A) Raman of ACNFs and ANHTGCNs. (B) N1 XPS spectra of ANHTGCNs. The N1 peak can be split into three Lorentzian peaks at ~ 398.6, 400.1, and 401.4 eV, representing pyridinic (N1), pyrrolic (N2), and graphitic (N3) type of N atoms. (C) EELS spectra of ANHTGCNs. (D) Pore-size distribution of ANHTGCNs calculated by applying a slit/cylindrical NLDFT model.

into the contracted Ni, resulting in the formation of a tunnel structure and graphitic carbon-coated Ni spheres (Figure 2E). The contraction shows that the increase of Ni surface energy cannot be compensated for by the energy obtained by binding the carbon to the Ni surface.[25] The driving force for the diffusion of Ni was the catalytic conversion of amorphous carbon into a more stable form of graphitic carbon at the reaction front.[26] The carbon atoms from the amorphous carbon (which is the carbon source) then diffused to the Ni part in contact with the graphitic carbon and the Ni atoms diffused to the amorphous carbon side,[25] which turned the amorphous carbon on the surface of Ni into graphitic carbon and created a hollow-tunnel structure (Figure 2F). When small Ni particles met, they coalesced. The diffusion of Ni particles ended when they met the stiff graphitic layers, producing larger Ni particles with a particle diameter ranging from 50 nm to 150 nm. The N-doped hollow-tunneled graphitic carbon/Ni nanofibers (NHTGCNNs) were thus prepared (Figure S4D). In the case of samples 2 and 3, there was sufficient time to gradually release the stress at the interfaces of the different phases by slowly sliding the flexible graphene sheets, leading to elastic deformation and keeping the graphitic layer intact.[24] No diffusion of Ni particles was observed. TEM and HRTEM images shown in Figure S2C, D† and Figure S5† indicate that the introduction of PMMA not only produced pores in the nanofibers, but also helped to dissolve the Ni nanoparticles. Pure N-doped hollow-tunneled graphitic carbon nanofibers (NHTGCNs) were thereby obtained. The low- and high- magnification TEM images in Figure 3A, B show that the activated materials possess a hollow structure. A selected area electron diffraction (SAED) pattern shows (Figure 3A, inset) ring-like patterns, suggesting that the synthesized carbon is graphitic. The HRTEM image in Figure 3C shows that the wall of the hollow structure consists of many defects between the discontinuous graphene sheets, as indicated by the arrows. The d-spacing of the graphene sheets in the nanofibers, corresponding to the (002) plane of the carbon, is in the range of 0.34-0.43 nm (Figure 3D).

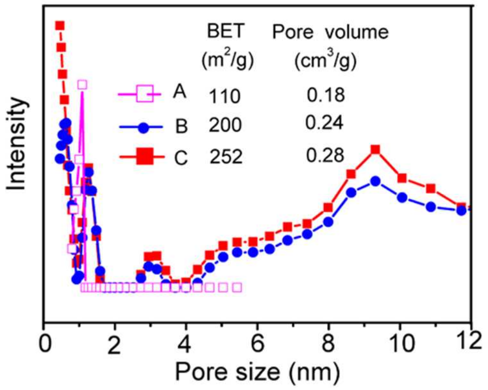

Figure 5. Pore size distribution of sample A by calcining PAN/Ni(Ac)$_2$ composite nanofibers, sample B by calcining PAN/PMMA/Ni(Ac)$_2$ composite nanofibers, and sample C from sample B after Ni diffusion.

The characterization of a sample of the ANHTGCNs by means of Raman scattering and X-ray photoelectron spectroscopy (XPS) is shown in Figure 4A, B. Comparison with ACNFs indicates that the G-band of the ANHTGCNs has a markedly enhanced intensity, with a ratio (R) of the intensity of the G-band to the intensity of the D-band (R = I_G/I_D) of 1.84, which is much higher than that of ACNFs (0.97). This finding indicates a great increase in the degree of graphitic crystalline structure owning to the use of Ni as a catalyst to promote the graphitization of carbon.[27] These results are consistent with the observations from the HRTEM. In the XPS N1s spectrum of the ANHTGCNs shown in Figure 4B, three components centered at ~ 398.6, 400.1, and 401.4 eV represent pyridinic (N1), pyrrolic (N2), and graphitic (N3) type N atoms, respectively.[28] A doping level of ~5 wt. % nitrogen in the graphitic porous carbon structure was determined. The N binding configuration includes 23.7 % pyridinic N, 52.2 % pyrrolic N, and 24.1 % graphitic N. The content of graphitic N in the ANHTGCNs is higher than that in ACNFs (7.7 %) (Figure S6A†). The electron energy loss spectroscopy (EELS) spectrum of the ANHTGCNs in Figure 4C shows a pre-peak of carbon at ~258 eV, which is attributed to the transitions to π* states in the sp^2 bonding carbon, suggesting the existence of graphene sheets in the prepared sample.[29] Complementary measurements were also arranged by XPS (further details can be found in Figure S6B†), and similar conclusions were reached. The surface and pore-size characterization of the ANHTGCNs was performed by nitrogen adsorption-desorption experiments. The specific Brunauer-Emmett-Teller (BET) surface area of the ANHTGCNs is 538 m^2 g^{-1} with a total pore volume of 0.77 m^3 g^{-1}, which is much higher than that of NHTGCNs (405 m^2 g^{-1}). Figure S7A† shows type IV isotherms with distinct hysteresis loops, which are characteristic of porous adsorption-desorption processes.[30] Figure 4D displays the results of a pore size analysis by applying a hybrid nonlocal density functional theory (NLDFT). It is evident that the ANHTGCNs possess micropores that peak at ~0.5, 0.6, 0.8, 1.3, and 1.5 nm, mesopores that peak at ~2.7, 3.2, 9, 25, and 40 nm, and macropores that peak at ~63 and 120 nm. To differentiate between the pores of different sizes formed by different mechanisms, more information about pore size distribution of controlled samples is studied. As shown in Figure 5 and Figure S7B†, it is very clear that introduction of PMMA produces four kinds of pores peaked at ~3.2, 9, 25 and 40 nm. The intensity of the peak of ~9 nm in sample C is higher than that of sample B, showing that the diameter of the tunnel structure is ~9 nm. The peaks below 2 nm are mainly due to defects caused by the carbonization of PAN.[30,34] Sample C shows higher sur-

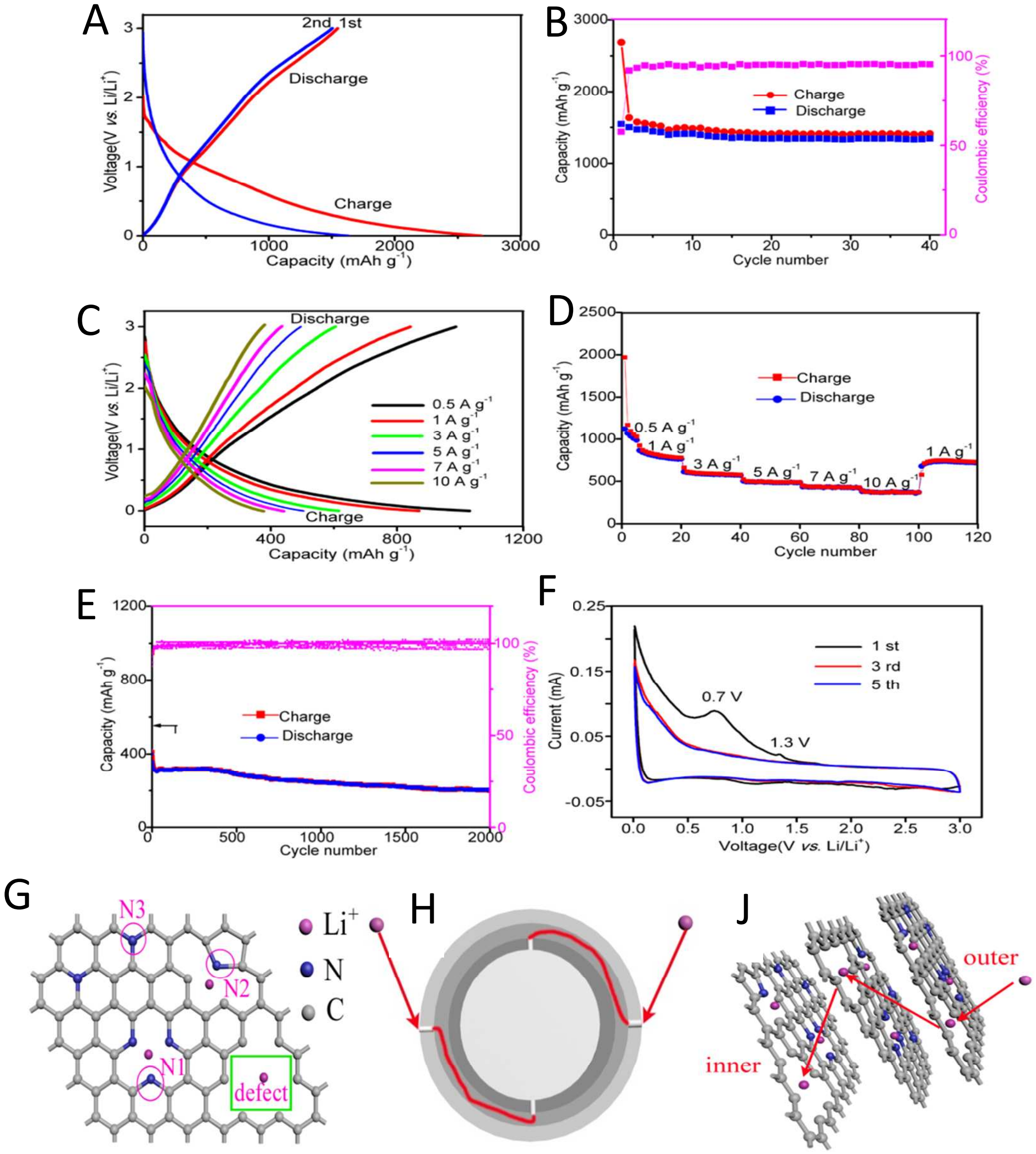

Figure 6. Electrochemical characteristics of ANHTGCNs tested between 3 and 0 V *versus* Li^+/Li. (A) Charge-discharge voltage profiles of ANHTGCN electrodes cycled at a current density of 0.1 A g^{-1}. (B, E) Cycling performance of ANHTGCNs electrodes at a current of (A) 0.1 A g^{-1} and (E) 10 A g^{-1}. (C, D) Galvanostatic charge-discharge profiles (C) and capacity (D) of ANHTGCNs cycled at various rates from 0.5 A g^{-1} to 10 A g^{-1}. (F) Cyclic voltammograms at a scan rate of 0.1 mV s^{-1}. (G-J) Schematic structure of N-doped graphene with defects (G) and illustrations (H, J) showing that lithium ions diffuse from outer space of ANHTGCNs into inner space of ANHTGCNs via the defected configuration.

face area of 252 cm^2/g and pore volume of 0.28 cm^3/g when compared to the samples A and B. And the large peaks at ~63 and 120 nm in the ANHTGCNs are caused by dissolving the Ni nanoparticles. The cumulative pore volume of the ANHTGCNs from pores smaller than 2 nm reaches ~42.4 % of the total pore volume (Figure S8B†). These results are consistent with the TEM and HRTEM observations.

Electrochemical performance

The N-doped ANHTGCNs with a high surface area and porous structure should display excellent electrochemical performance. Figure 6A shows the galvanostatic charge-discharge profiles of the

Table 1 Surface area, pore volume, R, and capacity at 0.1 A/g in different samples

	Surface area (m^2/g)	Pore volume (cm^3/g)	R = I_G/I_D	Capacity (mAh/g)
Sample 1	110	~0.18	~1.1	348
Sample 2	113	~0.18	~1.1	353
Sample 3	115	~0.18	~1.1	357
Sample 4	129	~0.21	~1.2	392
Sample 5	157	~0.26	~1.4	475

ANHTGCNs at a current density of 0.1 A g^{-1} in a voltage range of 0-3 V versus Li^+/Li. During the first cycle, the voltage plateau at ~0.7 V is ascribed to the formation of a solid electrolyte interface (SEI) and other side reactions.[31] The first reversible capacity is as high as 1546 mAh g^{-1}, which is ~4.2 times higher than the theoretical capacity of graphite (372 mAh g^{-1}). The volumetric capacity of the synthesized carbon electrode reaches ~1.8 Ah cm^{-3}. The large irreversible capacity of 1142 mAh g^{-1} in the initial cycle can be attributed to SEI formation.[16, 32] The cycling performance of the ANHTGCN electrodes is presented in Figure 6B, E. The capacity of the ANHTGCNs becomes stable and reversible after the first few cycles. The capacity remains ~1346 mAh g^{-1} at a current density of 0.1 A g^{-1} after 40 cycles and has only a little fading at a current density of 10 A g^{-1} after 2000 cycles. The coulombic efficiencies at both low and high current densities remain more than ~ 95% after the first few cycles. This performance is much superior to that of other carbon materials.[13, 14, 18, 19, 28] Figure 6F shows typical cyclic voltammograms of the ANHTGCN electrode. There are two reduction peaks of ~1.3 V and 0.7 V in the first cycle, corresponding to irreversible reactions between the ANHTGCN electrode and the electrolyte and co-intercalation of the solvated lithium ion into graphene sheets.[16, 17] During the third to fifth cycles, there is no clear change, demonstrating that the electrode is stable during the subsequent charge-discharge cycles. The ANHTGCNs also show an outstanding high-power rate capability. At current densities of 0.5, 1, 3, 5, 7, and 10 A g^{-1}, the reversible capacities of the ANHTGCNs are ~ 1000, 842, 605, 495, 435, and 380 mAh g^{-1}, respectively (Figure 6D). The morphology of the porous graphitic carbon becomes a little disorder and the crystallinity decreases after full lithiation (Figure S9A, B, E†). The wall of the porous structure shows more disordered graphene sheets and defects (Figure S9C†). Figure S9D† shows increased *d*-spacing distance of the (002) plane of the inter-wall carbon. The schematic illustrations in Figure 6G-J show that the lithium ions can diffuse from the outer space of the ANHTGCNs into the inner space of the ANHTGCNs through the defects. These results clearly demonstrate that lithium ions can rapidly reach the N-doped porous carbonaceous material, even at very high current rates. Additionally, the ANHTGCNs still have high capacities of ~876, 562, 421, 302, 248, 217 and 190 mAh g^{-1} at current densities of 0.1, 0.5, 1, 3, 5, 7 and 10 A g^{-1}, respectively, tested between 2 and 0 V *versus* Li^+/Li (Figure S10†). The low Coulombic efficiency for the ANHTGCNs electrodes in the first cycle (Figure 6A and Figure S10A†) can be enhanced by providing closed pores that only allow access of Li ions without the electrolyte, and creating a passivation layer on the surface of the mateial.[32] Table 1 shows surface areas, pore volumes, Rs, and capacities at 0.1 A/g in samples 1-5. It is clear that sample 5 shows higher surface area, pore volume, and degree of graphitic crystalline structure when compared to samples 1-3, further confirming the existence of the diffusion of Ni nanoparticles. Comparison of sample 4 to sample 5 shows that the large pressure difference enables better diffusion of Ni nanoparticles. Higher pore volume has improved capacity performance.

The exceptional electrochemical performance of the ANHTGCNs can be explained by their novel nanostructure and N-doping. Many defects caused by the formation of pyridinic and pyrrolic N in the ANHTGCNs can serve as Li storage sites and the Li ions can be adsorbed on the vacant sites induced by pyridinic and pyrrolic N.[19,33,34] The large *d*-spacing of the graphene layers not only stores Li ions in the regular sites of C_6Li, but also accommodates Li ions in neighboring sites, thus further enhancing the capacity.[35] The ample pores serve as reservoirs for the storage of Li ions as lithium clusters in pores, which can greatly improve the capacity performance. [9,16-18] The 1D nanostructure and high electrical conductivity of ANHTGCNs enable fast electron transport.[9] The large surface area provides a sufficient electrode/electrolyte interface for the absorption of Li ions and the increase of the rapid charge-transfer reaction.[11] The nanoscaled fibers and porous structure create short diffusion distances for fast lithium ion diffusion.[36] On the other hand, many defects in the ANHTGCNs allow the diffusion of Li ions from the outside carbon into the inner carbon, thus activating all of the carbon material. The N-doping of ANHTGCNs promotes electronic conductivity and electrochemical reactivity, further enhancing their excellent electrochemical performance.[20,]

Conclusions

In summary, controlled Ni-diffusion graphitization synthesis opens up a new path for the fabrication of polymer-based graphitic carbon nanofibers with a favorable nanostructure comprising N-doping, a high surface area, and a porous structure. The simple synthetic process can be extended to the fabrication of other nanostructured porous graphitic carbon materials, and even graphitic bulk carbon with a nanoporous structure. Our ongoing work shows that other metals (Fe and Co) and materials such as (polypyrrole and glucose) may also serve as catalysts and carbon sources. We anticipate that the resulting nanomaterials will make a decisive impact in a range of fields, such as sensors, electronic and electrochemical devices, catalysts, and hydrogen storage materials. The versatility and convenience of the synthesis process provide a new avenue for the rational engineering of N-doped nanoporous carbon materials.

Acknowledgements

The authors are grateful for the support received from the Research Grants Council of the Hong Kong Special Administration Region (grants: PolyU 5349/10E and PolyU 5312/12E) and the Hong Kong Polytechnic University (grants: G-YK47 and 1-BD08). We would like to thank Professor John. B Goodenough, University of Texas at Austin, for his valuable comments to this paper.

Notes and references

[a] Department of Mechanical Engineering, The Hong Kong Polytechnic University, Hong Kong, China.Tel: 852-2766 6663; Fax: 852-2365 4703 E-mail: mmlmzhou@polyu.edu.hk.
[b] School of Metallurgy and Environment, Central South University, Changsha, Hunan, China. E-mail: hncsyjy308@163.com.
[c] Department of Applied Physics and Materials Research Center, The Hong Kong Polytechnic University, Hong Kong, China.
[d] Centre for Advanced Materials Technology (CAMT), School of Aerospace, Mechanical and Mechatronics Engineering J07, The University of Sydney, NSW 2006, Australia.

† Electronic Supplementary Information (ESI) available: Detailed experimental methods, TEM, HRTEM, Nitrogen adsorption-desorption isotherms, XPS, and electrochemical performance. See DOI: 10.1039/b000000x/

1. A. Baji, Y.-W. Mai, S. C. Wong, M. Abtahi and X. S. Du, *Compos. Sci. Technol.,* 2010, **70**, 1401-1409.
2 J. Kong, N. R. Franklin, C. W. Zhou, M. G. Chapline, S. Peng, K. J. Cho and H. J. Dai, *Science,* 2000, **287**, 622-625.
3 H. X. Chang and H. K. Wu, *Energy Environ. Sci.*, 2013, *6*, 3483-3507.
4 Y. G. Li, W. Zhou, H. L. Wang, L. M. Xie, Y. Y. Liang, F. Wei, J. C. Idrobo, S. J. Pennycook and H. J. Dai, *Nature Nanotech.,* **2012**, *7*, 394-400.
5 G. H. Yu, L. B. Hu, M. Vosgueritchian, H. L. Wang, X. Xie, J. R. McDonough, X. Cui, Y. Cui and Z. N. Bao, *Nano Lett.,* 2011, **11**, 2905-2911.
6 A. C. Dillon, K. M. Jones, T. A. Bekkedahl, C. H. Kiang, D. S. Bethune and M. J. Heben, *Nature*, 1997, **386**, 377-379.
7 Y. H. Ng, S. Ikeda, M. Matsumura and R. Amal, *Energy Environ. Sci.*, 2012, **5**, 9307-9318.
8 B. Zhang, Y. Yu, Z. D. Huang, Y. B. He, D. Jang, W. S. Yoon, Y.-W. Mai, F. Y. Kang and J. K. Kim, *Energy Environ. Sci.*, 2012, **5**, 9895-9902
9 L. Qie, W. M. Chen, Z. H. Wang, Q. G. Shao, X. Li, L. X. Yuan, X. L. Hu, W. X. Zhang and Y. H. Huang, *Adv. Mater.,* 2012, **24**, 2047-2050.
10 J. W. Choi, J. McDonough, S. Jeong, J. S. Yoo, C. K. Chan and Y. Cui, *Nano Lett.,* 2010, **10**, 1409-1413.
11 Y. S. Hu, P. Adelhelm, B. M. Smarsly, S. Hore, M. Antonietti and J. Maier, *Adv. Funct. Mater.,* 2007, **17**, 1873-1878.
12 Y. Yu, L. Gu, C. B. Zhu, P. A. van Aken and J. Maier, *J. Am. Chem. Soc.,* 2009, **131**, 15984-15985.
13 L. W. Ji and X. W. Zhang, *Electrochem. Commun.,* 2009, **11**, 684-687.
14 L. W. Ji and X. W. Zhang, *Nanotechnology,* 2009, **20**, 155705-1557011.
15 L. L. Zhang, X. Zhao, M. D. Stoller, Y. W. Zhu, H. X. Ji, S. Murali, Y. P. Wu. S. Perales, B. Clevenger and R. S. Ruoff, *Nano Lett.,* 2012, **12**, 1806-1812.
16 Y. M. Chen, Z. G. Lu, L. M. Zhou, Y.-W. Mai and H. T. Huang, *Nanoscale,* 2012, **4**, 6800-6805.
17 Y. M. Chen, Z. G. Lu, L. M. Zhou, Y.-W. Mai and H. T. Huang, *Energy Environ. Sci.,* 2012, **5**, 7898-7902.
18 Z. J. Fan, J. Yan, T. Wei, G. Q. Ning, L. J. Zhi, J. C. Liu, D. X. Cao, G. L. Wang, F. Wei, *ACS Nano,* 2011, **5**, 2787-2794.
19 Z. S. Wu, W. C. Ren, L. Xu, F. Li and H. M. Cheng, *ACS Nano,* 2011, **5**, 5463-5471.
20 W. H. Shin, H. M. Jeong, B. G. Kim, J. K. Kang and J. W. Choi. *Nano Lett.,* 2012, **12**, 2283-2288.
21 D. Li and Y. N. Xia, *Nano Lett*., 2004, **4**, 933-938.
22 Y. J. Su, H. Wei, Z. Yang and Y. F. Zhang, *Carbon,* 2011, **49**, 3579-3584.
23 J. Chandra, D. Kandpal and B. R. K. Gupta, *Physica B,* 2009, **404**, 1087-1091.
24 M. K. Shin, B. Lee, S. H. Kim, J. A. Lee, G. M. Sinks, S. Gambhir, G. G. Wallace, M. E. Kozlov, R. H. Baughman and S. J. Kim, *Nat. Commun.,* 2012, **3**, 650.
25 S. Helveg, C. Lopez-Cortes, J. Sehested, P. L. Hansen, B. S. Clausen, J. R. Rostrup-Nielsen, F. Abild-Pedersen and J. K. Nørskov, *Nature,* 2004, **427**, 426-429.
26 R. Anton, *Carbon,* 2008, **46**, 656-662.
27 W. Gao, L. B. Alemany, L. Ci and P. M. Ajayan, *Nat. Chem.,* 2009, **1**, 403-408.
28 A. L. M. Reddy, A. Srivastava, S. R. Gowda, H. Gullapalli, M. Dubey and P. M. Ajayan, *ACS Nano,* 2010, **4**, 6337-6342.
29 R. R. Schlittler, J. W. Seo, J. K. Gimzewski, C. Durkan, M. S. M. Saifullah and M. E. Welland, *Science,* 2001, **292**, 1136-1139.
30 Y. W. Zhu, S. Murali, M. D. Stoller, K. J. Ganesh, W. W. Cai, P. L. Ferreira, A. Pirkle, R. M. Wallace, K. A. Cychosz, M. Thommes, D. Su, E. A. Stach and R. S. Ruoff, *Science,* 2011, **332**, 1537-1541.
31 L. G. Bulusheva, A. V. Okotrub, A. G. Kurenya, H. Zhang, H. Zhang, X. Chen and H. Song, *Carbon,* 2011, **49**, 4013-4023.
32 Y. M. Chen, X. Y. Li, K. S. Park, J. Song, J. H. Hong, L. M. Zhou, Y.-W. Mai, H. T. Huang and J. B. Goodenough, *J. Am. Chem. Soc.,* 2013, **135**, 16280-16283.
33. B. Zhang, Y. Yu, Z. L. Xu, S. Abouali, M. Akbari, Y. B. He, F. Y. Kang and J. K. Kim, *Adv. Energy Mater.,* 2013, DOI: 10.1002/aenm.201301448.
34. B. Zhang, Z. L. Xu, Y. B. He, S. Abouali, M. A. Garakani, E. K. Heidari, F. Y. Kang and J. K. Kim, *Nano Energy*, 2014, **4**, 88-96.
35 E. Yoo, J. Kim, E. Hosono, H. Zhou, T. Kudo and I. Honma, *Nano Lett.*, 2008, **8**, 2277-2282.
36 G.Q. Zhang, H. B. Wu, H. E. Hoster and X. W. Lou, *Energy Environ. Sci.*, 2014, **7**, 302-305.